High-acceleration Precision Point-to-Point Motion Control with Look-ahead Properties

Jianhua Wu, Zhenhua Xiong, Kok-Meng Lee, *Fellow, IEEE* and Han Ding, *Senior Member, IEEE*

Abstract— This paper investigates the effects of two control algorithms on high-performance point-to-point motions. The emphasis here is to overcome challenges in precision positioning of high-acceleration tables in the presence of significant external disturbances and exited vibration; an A-type of iterative learning control (ILC) algorithm for repetitive motions, and a look-ahead finite impulse response (FIR) filter plus sliding mode control for non-repetitive motions. The model-free convergence condition and the fastest-converging parameter equation for A-ILC are given in the frequency domain. Then, the FIR coefficients are decided through the ILC results and modified to eliminate the friction effect. Experimental studies demonstrate that both the algorithms perform well and the FIR-sliding mode control algorithm is robust in various experimental scenarios which include high acceleration (of $73.7 m/s^2$ or about 7.5 g), model parameters and disturbances deviations from the position, velocity and acceleration at which the ILC (and hence FIR) are trained.

Index Terms— linear motor, point-to-point motion, iterative learning control, FIR, high acceleration, look-ahead

I. INTRODUCTION

FAST point-to-point motions with high acceleration are often required in semiconductor industry; for example, wire bonding and die mounting. Many positioning tables driven by permanent-magnet (PM) based electromagnetic linear motor (EM-LM) are widely used to perform such motion tasks [1] because of their high force density, low thermal losses, high positioning accuracy and mechanical simplicity. EM-LM positioning tables, however, are very sensitive to external disturbance because they eliminate mechanical transmissions and directly connect with the load. To exploit the potential of EM-LM positioning tables, we explore advanced control techniques to achieve

high-performance point-to-point motions with emphases on overcoming challenges in controlling precision high-acceleration tables in the presence of significant external disturbances that reduce motion accuracy and exited vibration often resulting in long settling time.

Motivated by the needs in microelectronic industry where products have been continuously driven toward smaller feature size, faster speeds, and lower cost, a flurry of research has been devoted during the past two decades to developing advanced control algorithms such as motion profile generator, iterative learning control (ILC), finite impulse response (FIR) filter, and sliding mode control for high-acceleration point-to-point motions. Motion profile generator is an important factor to reduce the residual vibration caused by the high acceleration. Mizoshita *et al.* proposed a fifth-order polynomial profile generator [2], introducing the least vibration at the motion end. In order to minimize the residual vibration, Dijkstra *et al.* [3] used an iterative learning law to propose an optimal discrete time approach. Based on the conventional S-curve profile, Li *et al.* [4] used a level-shifted sinusoidal waveform to displace the step curve in the jerk profile, resulting in a smoother profile to cause little vibration at the motion end.

Besides the motion profile generator, high performance control algorithms are pivotal for high-acceleration point-to-point motions. Several controllers have been designed. Based on the known dominant vibrational modes, Singer *et al.* [5] proposed a FIR filter convolving with the control signals to cancel the vibration after half vibration period. In [6], Cheng *et al.* presented a composite nonlinear feedback controller (CNF) consisting of a linear feedback law (designed to yield a fast response) and a nonlinear feedback portion that gradually tunes the damping ratio to reduce the overshoot and vibration when the table approaches its destination. Wang *et al.* [7] proposed a soft variable structure controller (that makes the system eigenvalues tend toward negative infinity continuously as the table moves to its destination); under this controller, the table has a fast response of point-to-point motion. Hirose *et al.* [8] proposed a feedback plus a polynomial feedforward controller with coefficients optimized to provide the desired frequency shaping in the control signals for suppressing residual vibrations. In [9], a sampled-data polynomial was used in feedforward manner to deal with disturbances and vibrations. Kim *et al.* [10] used a sliding mode control algorithm with coefficients tuned through a disturbance observer to control point-to-point motions. Lai *et al.* [11] used two adaptive neural networks (NNs) to independently compensate the external vibration and friction disturbances for fast motion control.

Most prior studies primarily focused on exploring alternative controllers to suppress the effect of external

Jianhua Wu, Zhenghua Xiong and Han Ding are with the School of Mechanical Engineering, Shanghai Jiao Tong University, Shanghai, No.800, Dong Chuan Rd., Shanghai 200240, P. R. China (email: wujh@sjtu.edu.cn, mexiong@sjtu.edu.cn and hding@sjtu.edu.cn).

Kok-Meng Lee is with the Woodruff School of Mechanical Engineering, Georgia Institute of Technology, Atlanta, GA 30332-0405 USA, (email: kokmeng.lee@me.gatech.edu).

1

disturbances and/or vibration. Potsaid *et al.* [12] explored a sequence of control strategies, which began with an inverse model (as feedforward controller), next enhanced it utilizing a model-based ILC for repetitive motion, then replaced it with a FIR filter to approximating the ILC signals, and lastly adjusted the FIR coefficients using an adaptive law to make the table execute random motions. All the algorithms in [12] have the same feedback controller and modifications are primarily made in the feedforward (learning or adaptation) controller to compensate for the disturbances and eliminate the vibration. While the sequential approach is potentially useful, Potsaid *et al.* [12] carried out experiments on a laser scanning machine which had neither significant Coulomb friction nor other non-smooth nonlinearities.

Unlike most algorithms that calculate control signals based on current and past information of the motion profile to compensate or suppress the effect of external disturbances and vibration, this paper introduces a look-ahead property in designing the controller and offers the followings:

− Two point-to-point motion controllers are presented here for investigating the effects of the look-ahead property on high performance point-to-point motion; namely, a P+A-ILC for repetitive motions, and a FIR filter (approximating and replacing the ILC) with sliding mode control for non-repetitive motions. While extending the previous research on P+A-ILC [13] built upon [14] and [15] and on [16] where external disturbances are divided into linear and nonlinear components for convergence analysis, this paper gives the model-free convergence condition and the fastest-converging parameter equation. Additionally, a look-ahead FIR filter complemented by sliding mode control is utilized in the feedforward manner for random runs.

− The ILC and FIR control algorithms have been implemented on an EM-LM positioning table; and their effectiveness for controlling the high-acceleration point-to-point motion has been experimentally investigated against the basic cascaded P/PI feedback control structure. Four additional experimental studies were conducted to evaluate the effect of parameter variations on the robustness of the FIR filter with sliding mode control. The findings which include high acceleration (of 73.7m/s^2 or about 7.5g) demonstrate that the ILC-based FIR with sliding mode control performs well for non-repetitive motions and is robust in various experimental scenarios including model parameters and disturbances deviations from the position, velocity and acceleration at which the ILC (and hence FIR) are trained.

The two control strategies presented here have the advantages that they are easy to implement and require little information about the controlled model and the external disturbances. While illustrated in the context of an electromagnetic linear motor system, they can be applied to a broad spectrum of other PM-based actuator systems; for examples, multi-DOF spherical motors [17], mega-speed drive systems [18] and compliant micromanipulator [19].

II. POINT-TO-POINT MOTION CONTROLLER DESIGN

A. Controlled System Model of an EM-LM system

Fig. 1 shows a typical real-time motion control of an EM-LM which consists of a current, a velocity and a position loops with controllers $G_i(s)$, $G_v(s)$ and $G_x(s)$ respectively. In Fig. 1, $G_{p1}(s)$ and $G_{p2}(s)$ are the transfer functions correspond to the electrical and mechanical subsystems of the EM-LM, and $H(s)$ is a low-pass filter, and f_L is external load (disturbance). In this paper, we investigate the effects of point-to-point motion control of the position loop control algorithm with the plant dynamics mathematically characterized by the form suggested in (1):

$$X(s) = G(s)V_r(s) + D(s) \qquad (1)$$

where $X(s)$ and $V_r(s)$ are the Laplace transforms of the displacement $x(t)$ and velocity reference $v_r(t)$; and $G(s)$ and $D(s)$ can be derived from the block diagram:

$$G(s) = \frac{G_v G_i G_{p1} G_{p2}}{1 + G_i G_{p1} + G_v G_i G_{p1} G_{p2} H} \frac{1}{s} \qquad (1a)$$

$$D(s) = \frac{-(1 + G_i G_{p1}) G_{p2}}{1 + G_i G_{p1} + G_v G_i G_{p1} G_{p2} H} \frac{F_L}{s} \qquad (1b)$$

In (1a), (1b) and subsequent derivations, we denote the Laplace domain variables using capitalized letters and drop "(s)" for simplicity. The disturbance in (1b) is divided into two parts:

$$D(s) = D_r(s) + D_n(s) \qquad (2)$$

where $D_r(s)$ represents the repetitive disturbance; and $D_n(s)$ the non-repetitive disturbance.
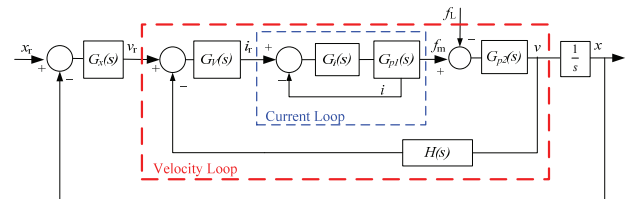

Fig. 1 Electromagnetic linear motor controlled system

B. Iterative Learning Control (ILC)

We first propose a proportional feedback controller plus a feedforward iterative learning control (ILC) in the position loop for repetitive motions. Fig. 2 illustrates the control diagram, where the control signal to the plant during the ith cycle is written as

$$v_{r,i}(t) = \hat{v}_i(t) + K_p e_i(t) \qquad (3)$$

where $e_i(t) = x_r(t) - x_i(t)$. In (3), the position-feedback controller $G_x(s)$ is proportional with gain K_p; and $\hat{v}_i(t)$ is the feedforward ILC effort:

$$\hat{v}_i(t) = \hat{v}_{i-1}(t) + k e_{i-1}(t + \tau) \qquad (4)$$

where k is a positive learning parameter; and τ is the look-ahead time.
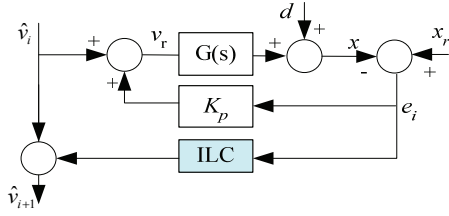
2

Fig. 2 Block diagram illustrating iterative learning control

We derive the convergence condition for the above controller that satisfies the following two assumptions:

Assumption 1: All operations start from the same initial conditions, $x_i(0)=x_r(0)$ for $i =1, 2...$ Any differences, however, can be treated as a non-repetitive disturbance.

Assumption 2: During the movement, the control signals do not saturate. This assumption can generally be satisfied by specifying proper motion profiles.

From (3), $\hat{v}_i = v_{r,i} - K_p e_i$. Substituting $\hat{v}_i(t)$ and $\hat{v}_{i-1}(t)$ from (3) into (4), the result in Laplace domain is given by (5):

$$V_{r,i} = V_{r,i-1} + ke^{\tau s}E_{i-1} + K_p(E_i - E_{i-1}) \quad (5)$$

Since $E_{i-1} - E_i = X_i - X_{i-1}$, and from (1) and (2)

$$X_i - X_{i-1} = G(V_{r,i} - V_{r,i-1}) + D_{n,i} - D_{n,i-1} \quad (6)$$

Equation (5) reduces to (7):

$$E_i = \frac{1+\left(K_p - ke^{\tau s}\right)G}{1+K_pG}E_{i-1} - \frac{D_{n,i} - D_{n,i-1}}{1+K_pG} \quad (7)$$

Through recursive analyses, (7) becomes

$$E_i = \hat{G}^{i-1}E_1 - \sum_{j=1}^{i}\left[\frac{\hat{G}^{j-1}}{1+K_pG}\left(D_{n,i+1-j} - D_{n,i-j}\right)\right] \quad (8)$$

where

$$\hat{G} = \frac{1+\left(K_p - ke^{\tau s}\right)G}{1+K_pG} \quad (8a)$$

The convergence for the ILC requires $|\hat{G}(j\omega)|<1$, which can be rewritten (by squaring both sides) yielding the convergence condition (9):

$$k|G(j\omega)| < 2K_p|G(j\omega)|\cos(\tau\omega) + 2\cos[\tau\omega + \angle G(j\omega)] \quad (9)$$

Theorem: *When the system (1) is under the control of (3) and (4), the tracking error converges if (9) holds.*

The proof of this theorem is given in Appendix A.

Remark 1: As differences in initial conditions for any cycle can be regarded as a non-repetitive external disturbance, deviations from *Assumption 1* will not cause the ILC to diverge provided the initial errors are small. Moreover, bounded initial errors result only in bounded tracking errors [13, 14].

Remark 2: Assumption 2 can generally be satisfied through specifying proper motion profiles. Even though the control effort is saturated, the above control algorithm can also achieve satisfactory performance as described

in [13].

Remark 3: The convergence condition (9) is simplified to

$$k < 2K_p\cos(\tau\omega) \quad \text{if} \quad K_p|G(j\omega)| \gg 1 \quad (10)$$

In other words, the algorithm parameters can be chosen independently on the controlled system model.

Remark 4: For specified constants (τ, K_p and k), the condition (10) cannot hold for all frequencies since $\cos(\tau\omega)$ may be negative. Thus, the signal should be cut off when $\omega \geq \omega_{off}$ where ω_{off} is a pre-defined cutoff frequency. On the other hand, excited vibrations (with $\omega < \omega_{off}$) will be compensated by the learning algorithm.

Remark 5: The fastest convergence occurs when $|\hat{G}(j\omega)|$ is a minimum. This is equivalent to

$$\frac{d\,|1+K_pG(j\omega) - ke^{j\tau\omega}G(j\omega)|^2}{dk} = 0 , \text{ which leads to}$$

$$k|G(j\omega)| = K_p|G(j\omega)|\cos(\tau\omega) + \cos[\tau\omega + \angle G(j\omega)] \quad (11)$$
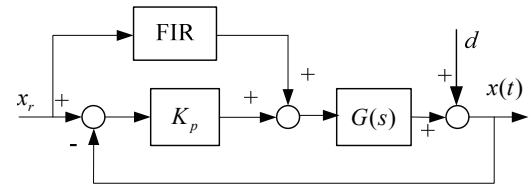
If $K_p|G(j\omega)| \gg 1$, (11) is simplified to

$$k = K_p\cos(\tau\omega) \quad (12)$$

C. Finite Impulse Response Filter with Sliding mode Control
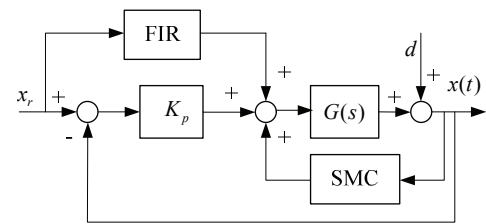
ILC is only suitable for repetitive motions and a number of trainings are needed to achieve a satisfactory performance. However, in practice, positioning tables often perform random runs. To allow for non-repetitive motions, we use a look-ahead finite impulse response (FIR) filter to displace ILC as shown in Fig.3 (a), which maps the reference command x_r to the feedforward control signals. The feedforward control signal at time k is parameterized by the FIR filter as follows

$$\begin{aligned}v_{fir}(k) &= w_1 x_{r,k-n_1+1} + w_2 x_{r,k-n_1+2}... + w_{n_1}x_{r,k}\\ &+ w_{n_1+1}x_{r,k+1} + ... + w_{n_1+n_2}x_{r,k+n_2}\end{aligned} \quad (13)$$

where $n = n_1 + n_2$ is the order of the filter; n_2 is the look-ahead horizon; and $W = \{w_i, i \in n\}$ are the coefficients.

(a) FIR

(b) FIR plus sliding mode control

Fig. 3 Block diagram

The filter coefficients $W = \{w_i, i \in n\}$ can be decided

3

through a least-square fit to the $(x_r, \hat{v})$ data obtained from the ILC results, i.e. set $v_{fir}(k) = \hat{v}_\infty(k)$. Write (13) in the matrix form as

$$\underbrace{\begin{bmatrix} v_{fir}(k_1) \\ \vdots \\ v_{fir}(k_l) \end{bmatrix}}_{V_{fir}} = \underbrace{\begin{bmatrix} x_{r,k_1-n_1+1} & \cdots & x_{r,k_1+n_2} \\ \vdots & \ddots & \vdots \\ x_{r,k_l-n_1+1} & \cdots & x_{r,k_l+n_2} \end{bmatrix}}_{X_r} \underbrace{\begin{bmatrix} w_1 \\ \vdots \\ w_{n_1+n_2} \end{bmatrix}}_{W} = \underbrace{\begin{bmatrix} \hat{v}_\infty(k_1) \\ \vdots \\ \hat{v}_\infty(k_l) \end{bmatrix}}_{\hat{V}_\infty} \quad (14)$$

where (k_1, k_l) is the range of data used for fit. The least square solution is

$$W = X_r^+ \hat{V}_\infty = \left(X_r^{'} X_r \right)^{-1} X_r^{'} \hat{V}_\infty \quad (15)$$

Remark 6: In (14) and (15), the subscribe ∞ means the ILC control signals in the infinite cycle. However, in implementations, the ILC control signals that perform satisfactorily are enough for the decision of the FIR coefficients.

Remark 7: The ILC feedforward control signals tend to compensate the external disturbances and excited vibrations. Thus (k_1, k_l) should include the complete transient motion, i.e. $(k_1, k_l) \supseteq (0, (T_f + \tau)/T)$. In implementations, $x_r(k) = 0$ for $k \le 0$ and $x_r(k) = s$ for $k > T_f/T$, where T is the sampling time; and T_f is the motion time as in (20).

Remark 8: Since the control signals depend on the table position, velocity and acceleration, the parameter n_1 must be equal to or larger than 3 to include the velocity and acceleration information. A heuristic condition to choose n_2 is that $n_2 T \ge \tau$ to include the look-ahead time in ILC.

Remark 9: The friction has a stick-slip effect causing non-zero control signals when the table positions at the destination in the ILC algorithm. Based on the ILC signals, (15) will induce a vector $\sum w_i \ne 0$ introducing a constant non-zero input into the system when the table positions at a non-zero target. That is, suppose the table is at the position s, then $v_{fir} = s \sum w_i \ne 0$ which can be regarded as a constant external disturbance and must be eliminated. In this paper, the FIR coefficients are modified as follows:

$$\hat{w}_i = w_i - \frac{w_i^2}{\sum w_k^2} \sum w_k \quad (16)$$

Obviously $\sum_{i}^{n} \hat{w}_i = 0$ and thus, the feedforward input vanishes at any constant position under the modified coefficients.

Remark 10: Equations (15) and (16) imply that the FIR coefficients obtained from the ILC results are constants, and produces fixed inputs once the motion profile is generated. Since FIR is utilized as a feedforward controller, stability is not an issue.

The FIR approximates the ILC algorithm closely. However, any small differences between ILC and FIR outputs may exist and degrade the point-to-point motion

performance. To compensate for this deviation the sliding mode control (well known for its effectiveness in system regulation [20-21]) is employed here to complement the FIR as shown in Fig.3 (b). To accomplish this objective, we define

$$p = \dot{e} + \lambda e \quad (17)$$

where $\dot{e} = \dot{x}_r - \dot{x}$ with $\dot{x}_r$ obtained from the motion profile from (20) and $\dot{x}$ obtained through numerical difference. The sliding mode control expression is
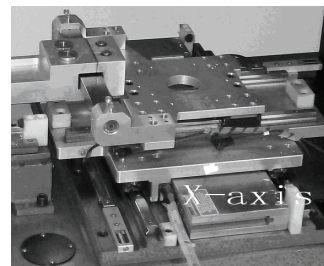
$$v_s = f_{max} sat(p/\delta) \quad (18)$$

where λ, f_{max} and δ are positive constant parameters, $sat(p/\delta) = sign(p) \min\{| p/\delta |, 1\}$. With the help of the above sliding mode control, position errors converge to a bounded layer. For readability, the (straightforward but lengthy and standalone) convergence analysis is detailed for interested readers in Appendix B so that the significance and contributions of experimental findings can be more clearly followed.

The FIR plus SMC structure compensates the model dynamics and repetitive disturbances using the FIR that approximates the ILC while suppressing non-repetitive disturbances by the feedback P controller and SMC to achieve perfect tracking. In order to achieve satisfactory performance by FIR plus SMC, the deviations of the model and disturbance dynamics between the ILC and the FIR plus SMC should be small; otherwise, the ILC must be re-trained, and the FIR parameters must then be determined from the new ILC results.
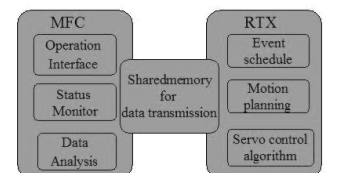
III. EXPERIMENTAL INVESTIGATION
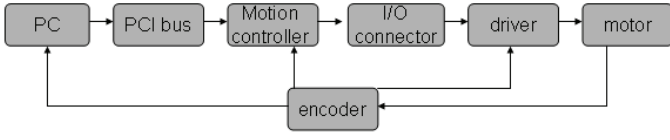
A. Positioning Table Experimental Setup

Fig. 4(a) shows a high-acceleration positioning table driven by a linear motor (Kollmorgen IL18-100A1P1) with a non-contact linear optical encoder (Heidenhain LIDA 475) for position feedback. The table sits on a pair of THK linear contact rails which inevitably bring frictions into the system. Other disturbances include cogging force and force ripples. All these disturbances vary with the position, velocity and acceleration of the table. The PC-based control hardware consists of a driver (Kollmorgen Servo Star CE06250), and a motion controller (GT400SV-PCI by Googol Technology) which commands the driver for positioning the table via PCI buses, and receives control signals via DAC I/Os (Fig. 4c).

(a) Positioning table   (b) Real-time operation system

(c) PC-based control hardware

Fig. 4 EM-LM driven positioning table experimental setup

A PC-based motion control program (written in C language with a sampling frequency of 1kHz) has been developed and implemented on a VenturCom real-time operation system consisting of two subsystems (MFC and RTX) with a shared memory as shown in Fig. 4(b). MFC provides a friendly human-computer interface and executes non real-time operations (such as monitoring and off-line analysis) while RTX (as a timer) undertakes real-time tasks including data acquisition for feedback as well as real-time computing, control and communication between the controller and the driver of the positioning table.

The control system is designed in a cascaded fashion which includes a current, velocity and position loops (Fig. 1). The velocity and current loops are realized in the driver, while the position control algorithm is implemented in RTX. The current-loop has a very small time constant as compared to that of the mechanical part; thus, its transfer function is approximated by a constant thrust coefficient k_f (i.e., $f_m \approx k_f i_r$). The dynamics of the electromagnetic linear motor (EM-LM) can be modeled by (19):

$$m\dot{v} + bv = k_f i_r - f_L \qquad (19)$$

where m is the moving mass; and b is the viscous friction coefficient. . The velocity-loop is controlled by a PI controller $G_v(s) = k_{vp}(1 + k_{vi}/s)$. The plant transfer function has the form given in (1), where

$$G(s) = \frac{k_{vp}k_f(s + k_{vi})}{ms^2 + bs + k_{vp}k_f(s + k_{vi})H(s)} \frac{1}{s} \qquad (19a)$$

and $$D(s) = \frac{-F_L s}{ms^2 + bs + k_{vp}k_f(s + k_{vi})H(s)} \frac{1}{s} \qquad (19b)$$

where $H(s)$ is a low-pass filter with the cutoff frequency 80Hz. The detailed derivation of (19a) and 19(b) is shown in Appendix C.

B. Experimental Results

The ILC and FIR control algorithms are implemented on the high-acceleration positioning table and experimentally evaluated against the basic cascaded P/PI feedback control structure. The motion profile (suggested in [2] for least vibrations at the motion end) was utilized as the reference command for analyzing the point-to-point motions:

$$x(t) = 6s\left[(t/T_f)^5 - 2.5(t/T_f)^4 + (5/3)(t/T_f)^3\right] \qquad (20)$$

where the travel distance s is 2mm; and the motion time T_f is 15ms. The highest acceleration and velocity are 50.12m/s^2 (5.2g) and 0.25m/s respectively. The values of the characteristic parameters used in the experimental evaluation are tabulated in Table 1. The results, which
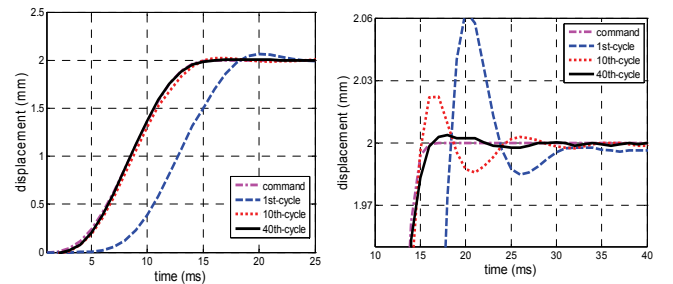
evaluate the performance in terms of tracking error, overshoot, and δ_s-stabilized time (defined as $\hat{t}_s = t_\delta - T_f$ where t_δ denotes the time after which the absolute positioning error is less than δ_s), are summarized in Figs. 5 and 6. In this paper, δ_s=5μm and $\hat{t}_s$ is referred to here as 5μm-stabilized time.

Table 1: Values of the parameters used experimental evaluation

EM-LM driven Table:

Peak force (N)	1200	Total movable mass, m (kg)	7.9
Continuous force (N)	270	Damping coefficient, b	87
Encoder precision (μm)	0.5	Thrust coefficient, k_f (N/A)	171
Sampling time T:	1ms		

Position and velocity controller gains: K_p=4000, k_{vp}=2000, k_{vi}=1000

ILC parameters: τ= 4ms, k=1000, cut-off frequency=50Hz

FIR Filter parameters: λ=1, δ=4μm, f_{max}=100; n_1=3, n_2=4.

$\mathbf{W}$ = $[-1.4113, 3.8634, -5.5677, -0.146, -2.0796, -0.8288, 6.1929]^T$

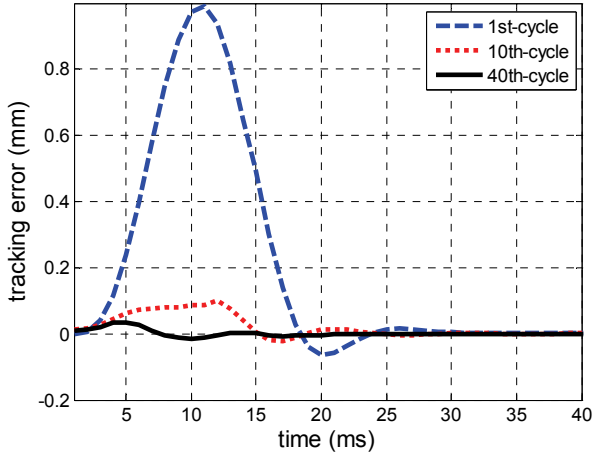$\hat{\mathbf{W}}$ = $[-1.4118, 3.8596, -5.5755, -0.146, -2.0807, -0.8289, 6.1833]^T$

Fig. 5 shows that the ILC tracking responses at 1st, 10th and 40th cycles, where the 1st cycle of the ILC is essentially the P controlled. Fig. 6(a) compares the ILC and FIR outputs with different look-ahead horizons. The FIR response and tracking error (at look-ahead horizon equal to 4) are graphed Figs. 6(b) and 6(c). Observations from these results are summarized as follows:

− In Fig. 5, the 1st-cycle response corresponding to the P-controlled position loop has three properties:
  a) It has a 4.5ms time-delay and thus a large tracking error (with maximum absolute error about 1mm).
  b) The maximum overshoot is 65μm (or 3.25%).
  c) It oscillates with a period of about 14ms resulting in a relatively long 5μm-stabilized time of 65ms with a steady-state position error of 5μm.

− As compared against the P controller (that alone cannot reduce the time-delay, vibration and steady-state error without sacrificing the 5μm-stabilized time and overshoot), the ILC eliminates the tracking errors and effectively reduces the 5μm-stabilized time and overshoot (Figs. 5a-c).

− Fig. 5(d) shows that the ILC converges pretty fast decreasing the maximum overshoot and 5μm-stabilized time to no more than 8μm (or 0.4%) and 3ms after 30 cycles. Similarly, the maximum tracking error is reduced from 1mm at the 1st cycle to 20μm after the 15th cycle.
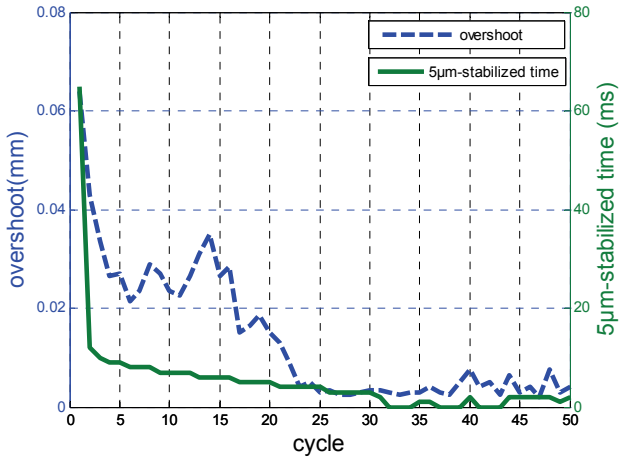

(a) ILC responses

(b) Zoom-in response around 2mm

(c) Tracking errors

(d) Overshoot and modified settling time

Fig. 5 ILC Tracking response (1st, 10th and 40th cycles)

(a) Comparison between ILC and FIR commands

(b) Zoom-in comparison among time interval [10, 20]ms

(c) Response curves

(d) Zoom-in response around 2mm

Fig. 6 FIR responses

– The effect of look-ahead horizons on the 7th order FIR output is illustrated in Fig. 6(a) and Table 2. The latter

tabulates the sum of squared deviation (SSD) between ILC and FIR showing that the FIR with a look-ahead horizon n_2 of 4 best approximates the ILC. As compared in Fig. 6(a), the control signal is oscillatory without the look-ahead horizon (n_2=0). Unlike the ILC control signal which does not vanish (but requires a relatively constant effort of 85) when the table reaches the positioning destination, the FIR control signal with modified coefficients equal to zero at the destination, as shown in the zoom-in plot Fig. 6(b).

– Figs. 6(c) and 6(d) show the FIR response curves. The overshoot is 12μm (or 0.6%) and the 5μm-stabilized time 2ms.

Table 2: Effect of look-ahead horizon on the sum of square deviation

Look-ahead horizon	0	1	2	3	4	5	6
SSD* ($10^5*(2^{-15}$m/s$)^2$)	425.7	118.3	20.4	3.7	3.0	3.0	4.1

C. Experimental Investigation of FIR Robustness

Five experimental studies were conducted to examine the effect of parameter variations on the robustness of the FIR filter:

Case 1: Effect of acceleration (Fig. 7)

The motion profile parameters are s=8mm and T_f=25ms corresponding to the highest acceleration of 73.7m/s^2 (about 7.5g) and velocity 0.6m/s.

Case 2: Effect of motion direction (Fig. 8)

The table moves from 0 to 2mm (with s=2mm and T_f=15ms), stays at 2mm until 200ms, and moves to −2mm (with s=4mm and T_f=20ms).

Case 3: Effect of cumulative motion (s=2mm and T_f=15ms)
   3a. Reciprocating motion (Fig. 9)
   3b. stair-like motion (Fig. 10)

Case 4: Effect of external impact disturbance (Fig. 11)

Since the motor driver has a closed architecture not accessible to users, the effect of an external disturbance on the control performance was simulated using an impact test (by striking the stage with a hammer). The motion profile parameters are s=2mm and T_f=15ms.

In Case 1 to Case 3, apart from disturbances in the system mentioned earlier, which include friction that varies with position and velocity, and the periodic cogging forces and force ripples, the motor parameters slowly change with position. There are also vibrations resulted from different accelerations. These external disturbances (friction, cogging force, force ripple and etc.) and slow parameter variations are position dependent. In experiments, the motions start at random positions with different trajectories (point-to-point lengths, velocities and accelerations) so that the FIR robustness can be evaluated by comparing the results of the above four cases (Figs. 7 to 10) against the base FIR response (Fig. 6):

– Case 1: Fig. 7(a) compares the response against the command curve. Since the results nearly overlap, Fig. 7(b) zooms in the detailed response at 8mm. Response has a maximum overshoot of 43.5μm (0.54%); and the 5μm-stabilized time is 5ms. The slightly higher

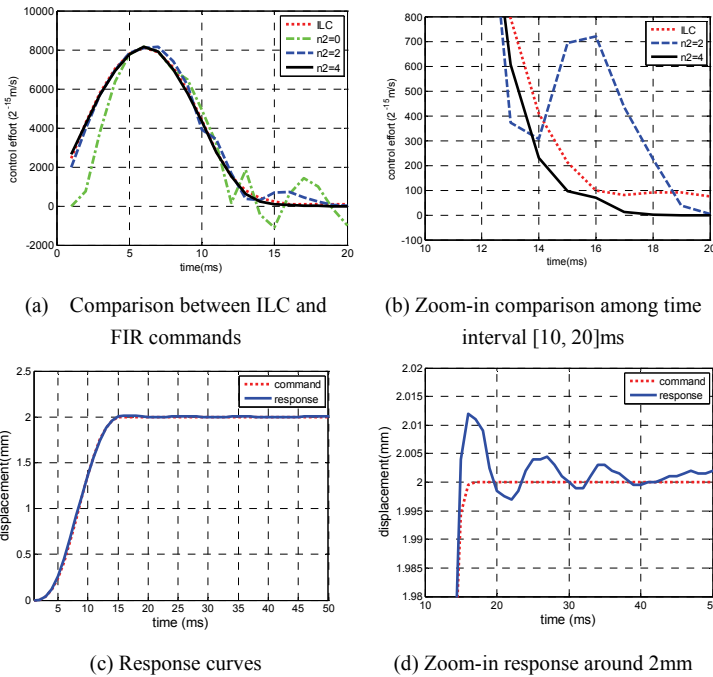5µm-stabilized time and maximum overshoot are due to the increase in motion acceleration and velocity.

− Case 2: Fig. 8(a) shows similar comparison with tracking errors given in Fig. 8(b). Figs. 8(c, d) display the zoom-in responses at 2mm and -2mm respectively. The maximum overshoots of the 2mm step-forward and 4mm step-backward motions are 4.5µm (0.225%) and 10.5µm (0.265%) respectively. The responses are nearly instantaneous (with 5µm-stabilized times of approximately 0ms and 1ms respectively).

− Case 3: Figs. 9 and 10(a) compare the responses of Case 3a and Case 3b against their respective command curves. Fig. 9(b) zoom-in the response of Case 3a around 2mm. Fig. 9(c) and Fig. 10(b) illustrate the 5µm-stabilized time and the overshoot of both cases. In these cumulative motion tests, the largest 5µm-stabilized time of Case 3b (stair-like) is 5ms larger than that of the 3ms of Case 3a (reciprocating). Case 3b also exhibits a larger maximum overshoot (15µm or 0.75%) than that of Case 3a (10.5µm). These results are somewhat expected since unlike the stair-like motion, the reciprocating motion stays within the range where learning (and thus FIR coefficients are based) takes place.

As demonstrated experimentally in Figs. 7 to 10, the non-repetitive motion responses nearly overlap follow the command curves non-distinguishably confirming that the ILC-based FIR algorithm with SMC is robust against disturbances and model deviations from the operating conditions at which the ILC (and hence FIR) are trained. As further demonstrated in Fig. 11 that compares the response (Case 4) against the command, the zoom-in detailed response (to an external impact disturbance) shows that the system is stable and the response converges to 2mm rapidly with 5µm precision.
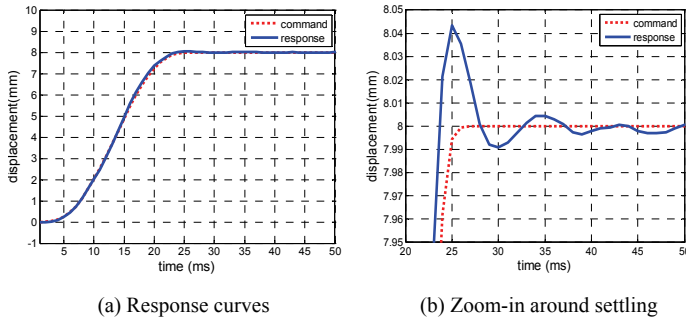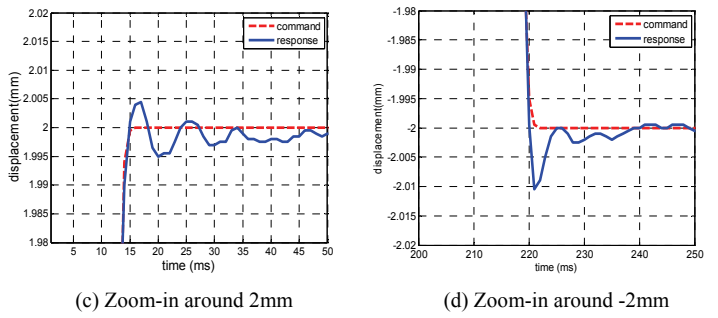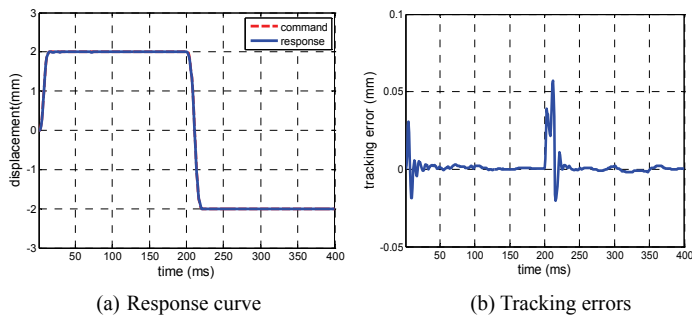

(c) Zoom-in around 2mm   (d) Zoom-in around -2mm

Fig.8 FIR response (Case 2)

(a) Response curves

(b) Zoom-in around 2mm

(c) Top: 5µm-stabilized time; bottom: overshoot

Fig. 9 FIR response (Case 3a)

(a) Response curves   (b) Zoom-in around settling

Fig. 7 FIR response Case 1

(a) Response curve   (b) Tracking errors

7

(a) Response curves

(b) Top: 5μm-stabilized time; bottom: overshoot

Fig. 10 FIR response (Case3b)

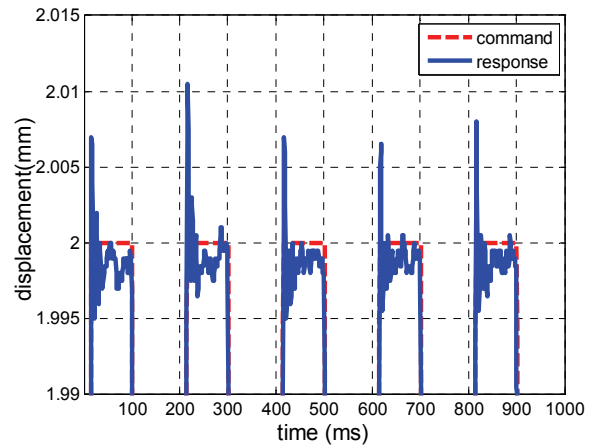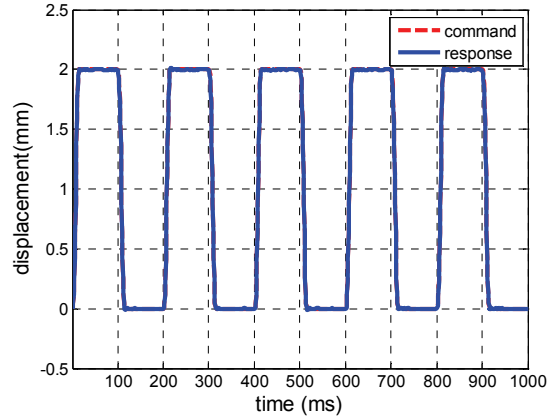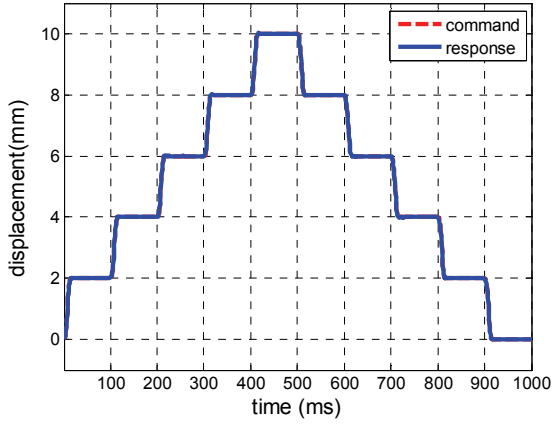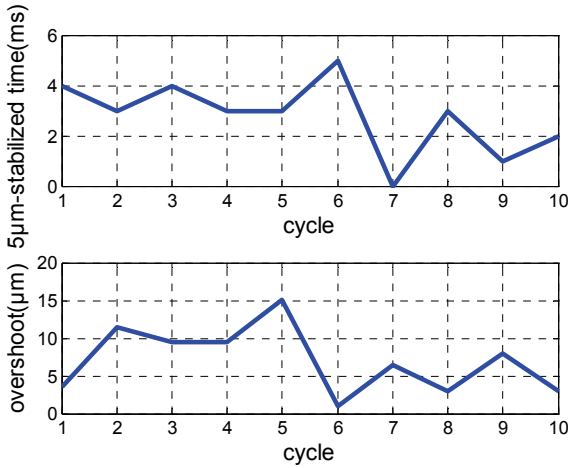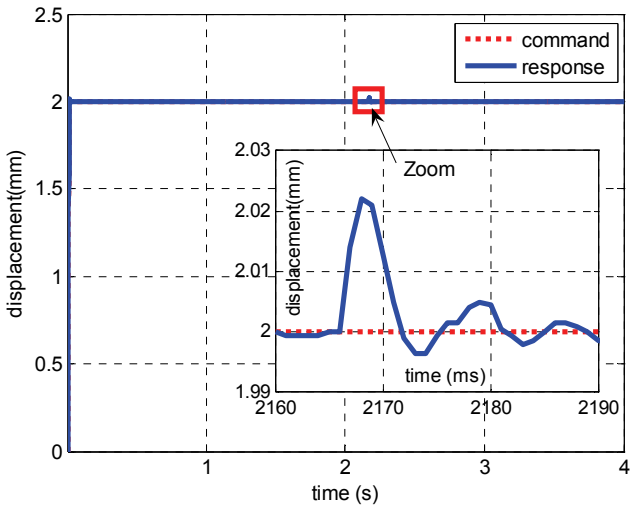Fig. 11 response under an impact disturbance by a hammer

IV. CONCLUSION

This paper proposes two high-performance point-to-point motion control algorithms. The first algorithm utilizes a feedback P-controller plus a feedforward A-type of ILC for repetitive motions. The convergence condition is given in frequency domain and

can be simplified to an inequality independent of the system model. Also the optimal learning parameter is found for the fastest convergence. The second algorithm is a look-ahead FIR filter (replacing the ILC for non-repetitive motions, where the filter coefficients are obtained from the ILC results and modified to eliminate the friction effect) with sliding mode control to compensate any deviation between FIR and ILC. Specifically, these two algorithms, which are easy to implement with a little information requirement for the controlled model and the disturbances, offer two novelties; 1) model-free convergence condition along with a fastest-converging parameter equation for the proposed ILC structure, and 2) FIR with a look-ahead property for approximating the ILC to cope with system dynamics, friction and other non-smooth nonlinear terms.

Experiments on a high acceleration positioning table driven by linear motors are carried out. The ILC converges pretty fast decreasing the maximum overshoot and 5μm-stabilized time to no more than 8μm (or 0.4%) and 3ms after 30 cycles with the maximal acceleration about $50.12 m/s^2$ (5.2g). Based on the ILC results, FIR plus sliding mode control performances non-repetitive motions well. Moreover, experiments on effects of larger acceleration (7.5g), motion direction and cumulative motion verify its robustness against parameter variations as well as illustrate the effectiveness.

Appendix A

Proof: From (7), the tracking error in the ith cycle contains two parts. The first part represents the $(i-1)^{th}$ cycle error and the second part is caused by non-repetitive disturbance. Since the non-repetitive disturbance accounts for only a small portion of the whole disturbances, it becomes very small after the suppression by the feedback controller. Therefore, this part can be omitted in the convergence analysis.

The convergence for (7) implies $|\hat{G}(j\omega)|<1$. Squaring both sides of (8a), it leads to

$$|1+(K_p - ke^{j\tau\omega})G(j\omega)|^2 < |1+K_pG(j\omega)|^2 \qquad (A-1)$$

That is

$$[1+(K_p - k\cos(\tau\omega) + jk\sin(\tau\omega))|G|(\cos\eta + j\sin\eta)]^2 \\ < [1+K_p|G|\cos\eta + jK_p|G|\sin\eta]^2 \qquad (A-2)$$

where $\eta = \angle G(j\omega)$.

Expanding both sides of (A-2), it becomes

$$k^2|G|^2 - 2|G|k\cos(\eta+\tau\omega) - 2|G|^2 K_p k\cos(\tau\omega) < 0 \qquad (A-3)$$

which equals to (9).

Moreover, similar to (7), we can get

$$E_{i-1}(s) = \hat{G}(s)E_{i-2}(s) - \frac{D_{n,i-1}(s) - D_{n,i-2}(s)}{1+K_pG(s)} \qquad (A-4)$$

Keep on this progress and finally we get

$$E_2(s) = \hat{G}(s)E_1(s) - \frac{D_{n,2}(s) - D_{n,1}(s)}{1+K_pG(s)} \qquad (A-5)$$

8

Combing (7), (A-4) and (A-5), it leads to (8). It suggests that the tracking error converges to a small bound as the cycle goes to infinite. And this bound is caused by the non-repetitive disturbances, which are suppressed by the feedback controller.

The proof is completed.

Appendix B

From Fig.3(b), the table output can be written as

$$x(t) = G(s)(K_p e(t) + v_{FIR} + v_s) + d(t) \qquad \text{(B-1)}$$

where v_{FIR} and v_s denote the output of the FIR and the sliding mode control respectively, $d(t)$ is the external disturbance corresponding to $D(s)$, $e(t) = x_r(t) - x(t)$ is the position error.

In repetitive motions, ILC achieve satisfactory performance by training through tracking error to compensate the model dynamics and repetitive disturbances. Hence, ILC affords the dominant control signals for the desired motion x_d. Since the FIR parameters are decided through the ILC control results, it is supposed that

$$G(s)v_{FIR} + d_r(t) = x_r(t) - \varepsilon(t) \qquad \text{(B-2)}$$

where $\varepsilon(t)$ is a small position error, and d_r is the repetitive disturbances. Substituting (B-2) to (B-1), we get

$$(K_p G(s) + 1)e(t) + G(s)v_s = \varepsilon(t) - d_n(t) \qquad \text{(B-3)}$$

where d_n is the small non-repetitive disturbances. From (18), it leads to

$$(K_p G(s) + 1)e(t) + G(s)f_{max} sat(p/\delta) = \varepsilon(t) - d_n(t) \qquad \text{(B-4)}$$

Three situations are discussed.
1. If $p > \delta$, (B-4) becomes

$$(K_p G(s) + 1)e(t) = \varepsilon(t) - d_n(t) - G(s)f_{max} \qquad \text{(B-5)}$$

Since $G(s)$ from (1) has an integral item, $G(s)f_{max}$ increases, then $e(t)$ will decrease and thus $\dot{e}(t) < 0$ until $p \leq \delta$.
2. If $p < -\delta$, (B-4) turns to

$$(K_p G(s) + 1)e(t) = \varepsilon(t) - d_n(t) + G(s)f_{max} \qquad \text{(B-6)}$$

Similarly, $e(t)$ will increase and thus $\dot{e}(t) > 0$ until $p \geq -\delta$.
3. If $-\delta \leq p \leq \delta$, substituting (17), (B-4) becomes

$$[1 + (K_p + \frac{f_{max}}{\delta}\lambda + \frac{f_{max}}{\delta}s)G(s)]e = \varepsilon(t) - d_n(t) \qquad \text{(B-7)}$$

$e(t)$ equals to the tracking error of $G(s)$ with the motion profile $\varepsilon(t) - d_n(t)$ under a PD controller whose parameters are $K_p + f_{max}/(\delta\lambda)$ and f_{max}/δ.

Situation 1 and 2 tell that p will converge to $[-\delta, \delta]$. Considering $v_{FIR}(t) = 0$ after $t > T_f$, $\varepsilon(t)$ becomes constant. If $d_n(t)$ is zero, from (B-7), $e(t)$ converges to a constant, i.e., $\dot{e}(t) \to 0$. Combing situation 1 and 2, the position error will converge to $[-\delta/\lambda, \delta/\lambda]$ at least. In real systems, $d_n(t)$ is usually not zero but a small value. Under the PD controller as in (B-7), the error will converge to a bounded layer.

Remark11: Because the FIR affords the dominant control signals for the point-to-point motion, only a small f_{max} is needed, which will not bring stability problem in the PD control in (B-7) and will not cause a violent chattering.

Appendix C

As mentioned above, the current loop transfer function in Fig.1 can be approximated by a constant thrust coefficient k_f and the mechanical subsystem G_{p2} has the following form

$$m\dot{v} + bv = f_m - f_L \qquad \text{(C-1)}$$

Combing $f_m \approx k_f i_r$, (C-1) gets to (19). Thus the transfer functions from i_r to v and from f_L to v are

$$G_{p2i} = \frac{V}{I_r} = \frac{k_f}{ms + b} \qquad \text{(C-2a)}$$

$$G_{p2L} = \frac{V(s)}{F_L(s)} = -\frac{1}{ms + b} \qquad \text{(C-2b)}$$

where V, I_r and F_L are the Laplace form of v, i_r and f_L respectively.

Under the velocity controller $G_v = k_{vp}(1 + k_{vi}/s)$ and the feedback filter H, the system can be written as

$$\frac{V}{V_r} = \frac{G_v G_{p2i}}{1 + G_v G_{p2i} H} = \frac{k_{vp} k_f (s + k_{vi})}{ms^2 + bs + k_{vp} k_f (s + k_{vi})H(s)} \qquad \text{(C-3a)}$$
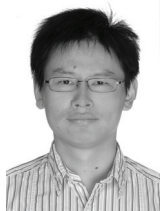
$$\frac{V}{F_L} = \frac{G_{p2L}}{1 + G_v G_{p2i} H} = \frac{-s}{ms^2 + bs + k_{vp} k_f (s + k_{vi})H(s)} \qquad \text{(C-3b)}$$

According to $X = V/s$ and (1), equations (19a) and (19b) are obtained.

Reference

[1] H. Ding and Z. Xiong, "Motion Stages for Electronic Packaging Design and Control," *IEEE Robot. Autom. Mag.*, vol. 13, no.4, pp. 51-61, Dec. 2006.

[2] Y. Mizoshita, S. Hasegawa, K. Takaishi, "Vibration Minimized Access Control for Disk Drives," *IEEE Trans. Magn.*, vol.32, no.3, Part 2, May, pp.1793-1798, 1996.

[3] B. Dijkstra, N. Rambaratsingh; C. Scherer, O. Bosgra, M. Steinbuch, and S. Kerssemakers, "Input Design for Optimal Discrete Time Point-to-point Motion of an Industrial XY-positioning table," in *Proc 39th IEEE Conf. Decision Control*, vol.1, pp.901- 906, 2000.

[4] H. Li, M. Le, Z. Gong and W. Lin, "Motion Profile Design to Reduce Residual Vibration of High-speed Positioning Stages", *IEEE/ASME Trans. Mechatronics*, vol.14, no.2, pp. 264-269, 2009.

[5] N. Singer and W. Seering. "Preshaping Command Inputs to Reduce Systems Vibration," *Trans. ASME, J. Dyn. Syst., Mea. Control*, vol. 112, no.1, pp: 76-82, 1990.

[6] G. Cheng, K. Peng, "Robust Composite Nonlinear Feedback Control with Application to a Servo Positioning System," *IEEE Trans. Ind. Electron.*, vol.54, no.2, pp.1132-1140, Apr., 2007.

[7] Y. Wang, Z. Xiong and H. Ding, "Fast Response and Robust Controller Based on Continuous Eigenvalue Configuration and Time Delay Control", *Robot. Comput. –Integr. Manuf.*, vol. 23, no.1, pp. 152-157, 2005.

[8] N. Hirose, M. Iwasaki, M. Kawafuku, H. Firal, "Deadbeat Feedforward Compensation with Frequency Shaping in Fast and Precise Positioning," *IEEE Trans. Ind. Electron.*, vol. 56, no. 10, pp: 3790-3797, Oct. 2009.

[9] T. Atrumi, "Feedforward Control Using Sampled-Data Polynomial for Track Seeking in Hard Disk Driver," *IEEE Trans. Ind. Electron.*, vol.56, no. 5, pp: 1338-1348, May, 2009.

[10] B.K. Kim, W.K. Chung, K. Ohba, "Design and Performance Tuning of Sliding-Mode Controller for High-Speed and High-Accuracy Positioning Systems in Disturbance Observer Framework," *IEEE Trans. Ind. Electron.*, vol.56, no. 10, pp: 3798-3809, Oct. 2009.

[11] C.Y. Lai, F.L. Lewis, V. Venkataraanan, X. Ren, S. Ge and T. Liew, "Disturbance and Friction Compensations in Hard Disk Drives Using Neural Networks", *IEEE Trans. Ind. Electron.*, vol.57, no. 2, pp: 784-792, Feb. 2010.

[12] B. Potsaid, J. Wen., M Unrath, D. Watt and M. Aplay, "High Performance Motion Tracking Control for Electronic Manufacturing", *Trans. ASME, J. Dyn. Syst., Mea. Control*, vol.129, no.6, pp.767-776, 2007.

[13] H. Ding, J. Wu, "Point-to-Point Motion Control for a High Acceleration X-Y Positioning Table via Cascaded Learning Schemes," *IEEE Trans. Ind. Electron.*, vol.54, no.4, pp.2753-2744, Oct. 2007.

[14] D. Wang, "On D-type and P-type ILC designs and anticipatory approach," *Int. J. Control*, vol.73, no.10, pp.890-901, 2000.

[15] D. Wang, Y. Ye, "Design and Experiments of Anticipatory Learning Control: Frequency-Domain Approach," *IEEE/ASME Trans on Mechatronics*, vol.10, no.3, pp.305-313, Jun. 2005.

[16] Z. Hu, D. Farson, "Design of a Waveform Tracking System for a Piezoelectric Actuator," *Proc. Inst. Mech. Eng. Part I-J Syst. Control Eng.*, vol. 222, no.1 pp.11-21,2008.

[17] H. Son, and K.-M. Lee, "Open-Loop Controller Design and Dynamic Characteristics of a Spherical Wheel Motor," *IEEE Trans. Ind. Electron.* vol. 57 no.10, pp. 3475-3484, 2010.

[18] C. Zwyssig, J. W. Kolar, and S. D. Round, "Megaspeed Drive Systems: Pushing Beyond 1 Million r/min," *IEEE/ASME Trans. on Mechatronics*, vol. 14 no.5, pp. 564 – 574, 2009.

[19] G. R. Jayanth and C.-H. Menq, "Modeling and Design of a Magnetically Actuated Two-Axis Compliant Micromanipulator for Nanomanipulation," *IEEE/ASME Trans. on Mechatronics,* vol.15, no.3, pp.360-370, 2010.

[20] X. Yu, O. Kaynak, "Sliding-Mode Control with Soft Computing: A Survey," *IEEE Trans. Ind. Electron.*, vol.56, no. 9, pp: 3275-3285, Sept. 2009.

[21] J. Zhang and Y. Xia, "Design of Static Output Feedback Sliding Mode Control for Uncertain Linear Systems", *IEEE Trans. Ind. Electron.*, vol.57, no. 6, pp: 2161-2170, June. 2010.

Jianhua Wu received his B.E. in Engineering Mechanics and his PH.D in Mechatronics in 2002 and 2007 respectively from Shanghai Jiao Tong University, Shanghai, China. He is now a lecture in the School of Mechanical Engineering, Shanghai Jiao Tong University. His current research interests focus on the high-speed and high-precision motion control, high performance motor driver design and servo self-tuning technology, which are applied to semiconductor manufacturing equipments and NC systems.

Zhenhua Xiong received the B.E. and M.E. degrees from the Department of Aircraft Design, Nanjing University of Aeronautics and Astronautics, Nanjing, China, in 1995 and 1998, respectively, and the Ph.D. degree in the EEE department from Hong Kong University of Science and Technology, in 2002. He is now an associate professor at the School of Mechanical Engineering, Shanghai Jiao Tong University. His research interests include motion control and electronics manufacturing.

Kok-Meng Lee (M'89–SM'02–F'05) received the B.S. degree from the State University of New York, Buffalo, in 1980, and the S.M. and Ph.D. degrees from Massachusetts Institute of Technology, Cambridge, in 1982 and 1985, respectively. He is currently a Professor in the Woodruff School of Mechanical Engineering, Georgia Institute of Technology, Atlanta. His current research interests include system dynamics/control, robotics, automation, and mechatronics. He holds eight patents in machine vision, 3-DOF spherical motor/encoder, and live-bird handling system. Prof. Lee is a Fellow of the American Society of Mechanical Engineers. He received the National Science Foundation Presidential Young Investigator Award, the Sigma Xi Junior Faculty Research Award, the International Hall of Fame New Technology Award, and the Kayamori Best Paper Award.

Han Ding (M'97–SM'00) received his Ph.D. degree from Huazhong University of Science and Technology (HUST), Wuhan, China, in 1989. Supported by the Alexander von Humboldt Foundation, he was with the University of Stuttgart, Stuttgart, Germany, from 1993 to 1994. He worked at the School of Electrical and Electronic Engineering, Nanyang Technological University, Singapore from 1994 to 1996. He has been a Professor at HUST ever since 1997. He is Director of State Key Lab of Digital Manufacturing Equipment and Technology at HUST. He is a "Cheung Kong" Chair Professor of Shanghai Jiao Tong University. He is now a Technical Editor of IEEE/ASME Trans. on Mechatronics. Dr. Ding serves as a guest editor and a technical committee member of semiconductor manufacturing automation in IEEE RA society. He acted as an Associate Editor of IEEE Transactions on Automation Science and Engineering from 2004 to 2007. He was a CASE Local Chair in 2006. He is the General Co-Chair for ICRA 2011. He has organized and chaired many technical sessions and workshops in various international conferences. His research interests include robotics, multi-axis machining and equipment automation.

10